A finite volume method for stochastic integrate–and–fire models

Fabien Marpeau, Aditya Barua and Krešimir Josić
Department of Mathematics, University of Houston, Houston, TX 77204-3008

September 26, 2008

Abstract. The stochastic integrate and fire neuron is one of the most commonly used stochastic models in neuroscience. Although some cases are analytically tractable, a full analysis typically calls for numerical simulations. We present a fast and accurate finite volume method to approximate the solution of the associated Fokker-Planck equation. The discretization of the boundary conditions offers a particular challenge, as standard operator splitting approaches cannot be applied without modification. We demonstrate the method using stationary and time dependent inputs, and compare them with Monte Carlo simulations. Such simulations are relatively easy to implement, but can suffer from convergence difficulties and long run times. In comparison, our method offers improved accuracy, and decreases computation times by several orders of magnitude. The method can easily be extended to two and three dimensional Fokker-Planck equations.

Keywords: stochastic integrate and fire model, numerical methods

1. Introduction

Over 100 years after its introduction in (Lapicque, 1907), the integrate and fire (IF) model remains one of the most ubiquitous models for simulating and analyzing the dynamics of neuronal circuits (Burkitt, 2006). The model offers a drastic simplification of the complex cellular processes by which a neuron processes incoming information (Rall, 1995; Tuckwell, 1988). However, despite its minimalistic nature, it captures some essential features of neuronal dynamics. Numerous variations of the model have been used to simulate single cell responses, as well as neuronal networks of a variety of shapes and sizes.

In the present work we consider a general IF neuron driven by a stochastic direct current input. This is a model of a neuron receiving a large number of weak synaptic inputs (Burkitt, 2006; Tuckwell, 1988). This is one of a few examples of an analytically tractable, stochastic model of a biophysical neuron, and has been successfully used to model and explain a number of phenomena experimentally observed in neural tissue (Brunel and Hakim, 1999; Doiron et al., 2003; Mattia and Del Giudice, 2004).

The behavior of a single IF model with stationary stochastic input is relatively well understood (Burkitt, 2006; Tuckwell, 1989). However, numerical simulations are still necessary in order to examine the validity of approximations used in cases that can be treated only perturbatively or are analytically intractable (Lindner and Schimansky-Geier, 2001; Brunel et al., 2001). While Monte Carlo (MC) methods are relatively easy to implement, determining convergence can be difficult, and run times can be prohibitive.

The goal of this paper is to present a finite volume method adapted to the IF model. The structure of this model offers unique challenges to the implementation of an accurate numerical method. To clearly explain the main problems in implementation and avoid burdensome notation, we consider a single neuron modeled by a one-dimensional stochastic differential equation. The advantages of the method become fully apparent when simulating small networks of neurons, and the extension of the present numerical schemes to the multidimensional setting is conceptually straightforward. A companion paper will therefore focus on the use of the method to examine the role of correlations in small networks of neurons.

An IF neuron with stochastic input is described by the Langevin equation:

$$\frac{dV}{dt} = f(V) + \sqrt{2D}\xi(t), \qquad V \in (-\infty, V^T). \tag{1}$$

When V reaches the threshold voltage, V^T, it is instantaneously reset to $V^R < V^T$. The threshold V^T marks the potential at which a stereotyped voltage transient (a spike) is initiated. This transient ends with the return to a lower, reset membrane potential V^R. We also include the possibility of a finite, absolute refractory period τ_R after V^T is reached. During this period a neuron is insensitive to inputs, and V is held fixed at V^R.

The function f which defines the deterministic (drift) behavior in Eq. (1) can take different forms. The numerical methods we present will work for a nearly arbitrary choice of f. We will consider the particular examples of the leaky integrate and fire model (LIF) where $f(V) = -V + \mu$, and the quadratic integrate and fire model (QIF) where $f(V) = (V - V_1)(V - V_2) + \mu$ (Ermentrout and Kopell, 1986; Latham et al., 2000). We take $\xi(t)$ to be a Gaussian stochastic processes with $\langle \xi(t) \rangle = 0$ and $\langle \xi(t)\xi(t') \rangle = \delta(t - t')$. However, extensions of the method to higher dimensions can be used to simulate models with colored noise, such as those in (Brunel and Latham, 2003; Rudolph and Destexhe, 2005; Lindner and Longtin, 2006).

We will describe a fast and accurate numerical method for computing the time dependent probability density, $P(t,V)$, of an ensemble of systems evolving according to Eq. (1). Therefore, $P(t,v)\Delta V$ is the approximate probability that $V \in (v, v + \Delta V)$ at time t. This density satisfies the Fokker-Planck equation in one space dimension (Risken, 1989; Gardiner, 1985):

$$\partial_t P(t,V) + \partial_V \big(f(V)P(t,V) - D\partial_V P(t,V) \big) = 0, \qquad V \in (-\infty, V^T) \backslash V^R. \tag{2}$$

For the purposes of the numerical simulation we restrict the equation to a finite domain (V^∞, V^T), where $V^\infty \ll V^R$. Since we want the total probability mass to be preserved, we assume a reflecting boundary condition at V^∞. The reset condition at V^T translates into an absorbing boundary condition, so that at the boundaries the solution satisfies

$$f(V^\infty)P(t,V^\infty) - D\partial_V P(t,V^\infty) = 0, \qquad \text{reflecting b.c. at } V^\infty \tag{3}$$

$$P(t,V^T) = 0 \qquad \text{absorbing b.c. at } V^T. \tag{4}$$

The density that crosses the threshold is being re-injected at V^R after a refractory period τ_R. This implies the following *interior* conditions

$$\big[P(t,V^R)\big] = 0, \qquad \text{continuity of } P(t,V), \tag{5}$$

$$\big[D\partial_V P(t,V^R)\big] = D\partial_V P(t - \tau_R, V^T), \qquad \text{influx of neurons that crossed } V^T \text{ at } t - \tau_R, \tag{6}$$

when $t \geq \tau_R$. The brackets denote jump discontinuities, so that $\big[\xi(t,z)\big] = \lim_{\substack{z^+ \to z \\ z^+ > z}} \xi(t,z^+) - \lim_{\substack{z^- \to z \\ z^- < z}} \xi(t,z^-)$. The initial probability density is an arbitrary non-negative function $P(0,V) = P_0(V)$ in (V^∞, V^T), such that $\int_{V^\infty}^{V^T} P_0(V)\, dV = 1$. As the diffusive flux at the threshold, $-D\partial_V P(t - \tau_R, V^T)$, is being re-injected in the interior according to Eq. (6), it is straightforward to observe that P satisfies the mass balance property:

$$\|P(t,.)\|_{L^1(V^\infty, V^T)} = 1 + \int_{\max(0, t-\tau_R)}^{t} D\partial_V P(s, V^T)\, ds\,. \tag{7}$$

We note that the partial differential equation described here has also been used to model the behavior of a population of neurons (Renart et al., 2004; Mattia and Del Giudice, 2002).

The accurate handling of boundary conditions is one of the most challenging problems in scientific computing. Improper discretization can lead to inaccuracy and instability. In the present case, boundary and interior conditions (5 –6) play an even more important role as they induce a re-injection of the probability mass inside the domain. Any error at the boundary can therefore easily propagate into the interior of the domain and affect the accuracy of the results globally.

A further challenge is the presence of the drift term $\partial_V \big(f(V)P(t,V) \big)$ in Eq. (2) which makes it difficult to obtain numerical densities that are accurate, stable and do not exhibit spurious oscillations. Improper

discretization of this term can result in large errors in the solutions. We therefore use an operator splitting technique that treats the drift operator separately from the rest of the equation.

For the purpose of discretizing the various mass transfers imposed by drift, diffusion and threshold/reset condition, the use of a finite volume methods is appropriate. Such methods enable us to control directly the flux of mass between the mesh elements. While finite element methods have been applied in the case of phase oscillator (Galán et al., 2007), they would need to be extended to handle the more complex boundary conditions of the LIF model. Finite difference schemes lack convenience on variable size meshes, and would be more difficult to apply.

To the best of our knowledge, condition (6) and the effects of a refractory period have not been approximated before by difference numerical schemes in this setting. A numerical scheme that employs operator splitting has been applied to a related model by (Apfaltrer et al., 2006). They considered a drift process with random jumps rather than diffusion, with inhibition modeled by mean field approximation. In contrast to our method, this approach does allow for large unitary events. Our approach employs an explicit method for the drift and an implicit method for the diffusion term, while only implicit methods were used by (Apfaltrer et al., 2006). We also extend these ideas with several analytical results about the stability properties of the algorithm. While some of the numerical difficulties are similar, the boundary conditions in that case are very different.

The code described here is available on SOURCEFORGE.NET at http://neuro-fvif.sourceforge.net/neuro-fvif.tar.gz

2. Methods

We give a detailed description of a numerical scheme to approximate the solution of system (2–6). The scheme results in probability densities that satisfy three main requirements: accuracy, nonnegativity and a discrete version of the mass balance property (25). Moreover, the simulation time is fast compared with MC simulations.

The main numerical difficulties are posed by the presence of the drift term $\partial_V\big(f(V)P(t,V)\big)$ in Eq. (2), and the threshold/reset conditions (5–6). The drift operator is isolated by splitting Eq. (2) into two parts (Strang, 1968; Toro, 2001)

$$\partial_t P + \partial_V(fP), \;=\; 0 \tag{8}$$

$$\partial_t P - D\partial_V^2 P \;=\; 0. \tag{9}$$

The time interval $\mathbb{R}_+$ on which the solution will be approximated is partitioned into subintervals (t_n, t_{n+1}). The time steps are defined by $\Delta t_n = t_{n+1} - t_n$, with $\Delta t = \max_n \Delta t_n$. We will denote the numerically obtained approximation of the solution at time t_n by P^n. Then P^{n+1} is obtained from P^n by using the splitting algorithm

$$P^{n+1} = \mathscr{S}_2\big(\mathscr{S}_1(P^n)\big)\ , \tag{10}$$

where $\mathscr{S}_1$ and $\mathscr{S}_2$ are approximation schemes for (8) and (9) respectively, along with split boundary and interior conditions specified later. This technique allows us to develop specific numerical schemes which are adapted to each differential operator in Eq. (2). The maximum time step Δt is restricted by a Courant-Friedrichs-Lewy (CFL) condition (Courant et al., 1928; Godlewski and Raviart, 1990) which provides stability of the explicit scheme $\mathscr{S}_1$ by ensuring that the drift term does not shift the numerical solution by more than one mesh per time step (Godlewski and Raviart, 1990). The scheme $\mathscr{S}_2$ is implicit and will remain stable under any time step. The details of the discretization are specified below.

The domain (V^∞, V^T) is split into N subintervals $Q_i = (V_{i-\frac{1}{2}}, V_{i+\frac{1}{2}})$ of size $\Delta V_i = V_{i+\frac{1}{2}} - V_{i-\frac{1}{2}}$, for $1 \le i \le N$. The meshpoints V_i are the centroids of the subintervals, $V_i = V_{i-\frac{1}{2}} + \frac{1}{2}\Delta V_i$, and we make sure that there

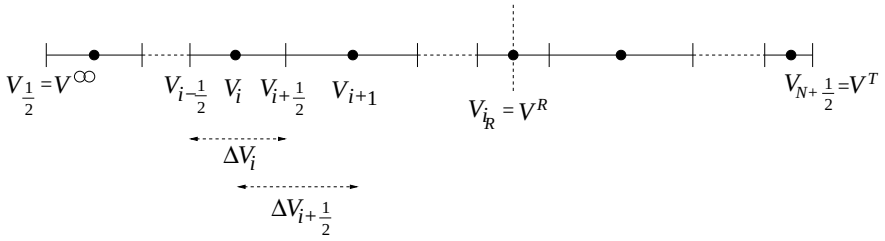

Figure 1. A schematic depiction of the subdivision of the domain (V^{∞},V^T) into subintervals $Q_i=(V_{i-\frac{1}{2}},V_{i+\frac{1}{2}})$. The centroid of interval Q_i is denoted V_i. The reset voltage V^R is at V_{i_R}.

exits an index i_R such that $V_{i_R}=V^R$, which means, one of our meshpoints, V_{i_R}, falls exactly on the reset potential. The distance between two meshpoints is defined by $\Delta V_{i+\frac{1}{2}}:=V_{i+1}-V_i$ (see Fig. 1).

We also use the following notational conventions: For any function h defined on (V^{∞},V^T) we denote by h_i^n either the approximation of the subinterval average $\frac{1}{\Delta V_i}\int_{Q_i}h(t,V)\,dV$ if h is an unknown, or the exact value when h is a known function. Let h^n denote the sequence $\{h_i^n\}_i$, and its discrete l^1– and l^∞–norms be defined by $\|h^n\|_{l^1}=\sum_{i=1}^N\Delta V_i|h_i^n|$ and $\|h^n\|_{l^\infty}=\max_i|h_i^n|$. Let $\Delta P_{i+\frac{1}{2}}^n:=P_{i+1}^n-P_i^n$, and lastly, the positive and negative part of any real number u are denoted $u^+=\max(0,u)$ and $u^-=\min(0,u)$ respectively.

2.1. Treatment of the drift operator: scheme $\mathscr{S}_1$

We first describe a conservative finite volume method to discretize the drift component defined in Eq. (8). The approximation of the cell-average solution of (8) at time t_{n+1} obtained in the first step, $\mathscr{S}_1$, is denoted $P_i^{n+\frac{1}{2}}$. Similarly, the approximation after the second step, $\mathscr{S}_2$, is denoted P_i^{n+1}.

A compromise between accuracy, nonnegativity and stability of our numerical densities is ensured by using flux limiters on an unstable high resolution numerical scheme (See (Harten, 1983; Sweby, 1984; Godlewski and Raviart, 1990; Bruneau et al., 2005; Marpeau and Saad, 2007)). We adapt this approach to non-constant meshes. Assuming that P^n is given, we define the numerical solution of (8) by

$$P_i^{n+\frac{1}{2}}=P_i^n-\frac{\Delta t}{\Delta V_i}(\mathscr{A}_{i+\frac{1}{2}}^n-\mathscr{A}_{i-\frac{1}{2}}^n). \tag{11}$$

The numerical fluxes $\mathscr{A}_{i+\frac{1}{2}}^n$ are approximations of $f(V_{i+\frac{1}{2}})P(t_n,V_{i+\frac{1}{2}})$ at the interfaces $V_{i+\frac{1}{2}}$. For all $i\neq 0,N,i_R,i_R-1$, we define the numerical fluxes by

$$\mathscr{A}_{i+\frac{1}{2}}^n=f_{i+\frac{1}{2}}^+P_i^n+f_{i+\frac{1}{2}}^-P_{i+1}^n+\frac{1}{2}\frac{\Delta P_{i+\frac{1}{2}}^n}{\Delta V_{i+\frac{1}{2}}}\Big(f_{i+\frac{1}{2}}^+(\Delta V_i-\Delta t\,f_{i+\frac{1}{2}}^+)\phi_{i+\frac{1}{2}}^p-f_{i+\frac{1}{2}}^-(\Delta V_{i+1}-\Delta t\,f_{i+\frac{1}{2}}^-)\phi_{i+\frac{1}{2}}^m\Big). \tag{12}$$

The flux-limiter coefficients $\phi_{i+\frac{1}{2}}^p$ and $\phi_{i+\frac{1}{2}}^m$ are defined by

$$\phi_{i+\frac{1}{2}}^p=\varphi\big(r_{i+\frac{1}{2}}^p,\frac{\Delta V_{i+\frac{1}{2}}}{\Delta V_i}\big),\qquad \phi_{i+\frac{1}{2}}^m=\varphi\big(r_{i+\frac{1}{2}}^m,\frac{\Delta V_{i+\frac{1}{2}}}{\Delta V_{i+1}}\big),$$

where

$$r_{i+\frac{1}{2}}^p=\frac{f_{i-\frac{1}{2}}^+\Delta P_{i-\frac{1}{2}}^n}{f_{i+\frac{1}{2}}^+\Delta P_{i+\frac{1}{2}}^n},\qquad r_{i-\frac{1}{2}}^m=\frac{f_{i+\frac{1}{2}}^-\Delta P_{i+\frac{1}{2}}^n}{f_{i-\frac{1}{2}}^-\Delta P_{i-\frac{1}{2}}^n},$$

and φ is a nonnegative function to be determined in order to provide stability of the numerical scheme (11) in the sense of Proposition 1. Indeed, if $\varphi \equiv 0$ is used, formula (12) reduces to the stable upwind flux, first order accurate, while $\varphi \equiv 1$ yields a centered scheme, which is more accurate but known to be unstable. A way to obtain stability is to use a function satisfying

$$0 \leq \varphi(a,b) \leq 2b \max\big(0, \min(1,a)\big) \text{ for all } (a,b) \in \mathbb{R} \times \mathbb{R}_+ \,. \tag{13}$$

In our numerical applications, we define a variant of the Superbee limiter (Roe, 1984),

$$\varphi(a,b) = 2b \max\big(0, \min(1,2a), \min(a,2)\big) \,, \tag{14}$$

which makes (11–12) stable while preserving a high accuracy (see appendix A). The main properties of $P^{n+\frac{1}{2}}$ are given in the next proposition.

PROPOSITION 1. *Under the* CFL *conditions*

$$\Delta t \Big(\frac{f^+_{i-\frac{1}{2}} - f^-_{i+\frac{1}{2}}}{\Delta V_i} + \Big(\frac{f_{i+\frac{1}{2}} - f_{i-\frac{1}{2}}}{\Delta V_i} \Big)^+ \Big) \leq 1 \,, \tag{15}$$

$$\Delta t \frac{|f_{i+\frac{1}{2}}|}{\min(\Delta V_i, \Delta V_{i+1})} \leq 1 \,, \tag{16}$$

the numerical scheme given in Eq. (11) together with the numerical flux defined in Eq. (12) is nonnegativity preserving and l^∞ stable in the following sense: For all $1 \leq i \leq N$ such that $i \neq 1$, $i \neq N$, $i \neq i_R$,

$$0 \leq P_i^{n+\frac{1}{2}} \leq \|P^n\|_{l^\infty} - \Delta t P_i^n f_i' \,. \tag{17}$$

REMARK 1. Notice that property (17) allows for exponential growth or decay of $\|P^{n+1}\|_{l^\infty}$, when the drift term is either compressive or expansive. However, when f is constant, Eq. (17) is the usual stability condition for advection equations.

Conditions (15–16) are automatically satisfied under the classical but more restrictive condition (for a general reference see (Barth and Ohlberger, 2004))

$$\frac{\Delta t}{\Delta V_i} (|f_{i+\frac{1}{2}}| + |f_{i-\frac{1}{2}}|) \leq 1 \,.$$

2.2. TREATMENT OF THE DIFFUSION OPERATOR: SCHEME $\mathscr{S}_2$

We use an implicit conservative finite volume method to discretize the diffusion equation (9), while preserving stability and positivity of the initial condition with no restriction on the time step. Integrating Eq. (9) over (t_n, t_{n+1}) in time and Q_i in space for $i \neq i_R$, we obtain

$$\int_{Q_i} P(t_{n+1},V)\,dV - \int_{Q_i} P(t_n,V)\,dV - \int_{t_n}^{t_{n+1}} D\partial_V P(t,V_{i+\frac{1}{2}}) - D\partial_V P(t,V_{i-\frac{1}{2}})\,dt = 0 \,. \tag{18}$$

Assuming that the approximations, $P_i^{n+\frac{1}{2}}$, of $\frac{1}{\Delta V_i}\int_{Q_i} P(t_n,V)\,dV$ have been determined in the previous step, $\mathscr{S}_1$, we define an implicit scheme approximating (9) as

$$\Delta V_i P_i^{n+1} - \Delta t(\mathscr{B}^{n+1}_{i+\frac{1}{2}} - \mathscr{B}^{n+1}_{i-\frac{1}{2}}) = \Delta V_i P_i^{n+\frac{1}{2}}. \tag{19}$$

Here for all i, $\mathscr{B}_{i+\frac{1}{2}}^{n+1}$ is a centered approximation of the diffusive flux $D\partial_V P(t,V_{i+\frac{1}{2}})$:

$$\mathscr{B}_{i+\frac{1}{2}}^{n+1} := D\frac{P_{i+1}^{n+1}-P_i^{n+1}}{\Delta V_{i+\frac{1}{2}}}\ . \tag{20}$$

2.3. Treatment of the boundary and internal conditions (3–6)

The boundary conditions at V^∞, and V^T are easily handled. One of the main novelties of the method is the treatment of the interior conditions given by Eqs. (5–6).

The reflecting boundary condition given in Eq. (3) is approximated by imposing $\mathscr{A}_{\frac{1}{2}}^n = 0$, $\mathscr{B}_{\frac{1}{2}}^{n+1} = 0$. Similarly, the absorbing boundary condition at V^T specified by Eq. (4) is approximated by $\mathscr{A}_{N+\frac{1}{2}}^n = 0$, and

$$\mathscr{B}_{N+\frac{1}{2}}^{n+1} = D\frac{P(t_{n+1},V^T)-P_N^{n+1}}{\Delta V_N/2} = -2D\frac{P_N^{n+1}}{\Delta V_N}\ . \tag{21}$$

The internal conditions are handled as follows: Eq. (5) implies continuity of the advective flux fP at the reset potential V^R. We keep the numerical fluxes $\mathscr{A}_{i_R\pm\frac{1}{2}}^n$ unchanged because Eq. (8) then holds in the entire domain.

However, the jump condition (6) is more difficult to discretize as it implies that the diffusion equation (9) does not hold in the entire domain and the discretization defined by Eq. (19) cannot be used. Integrating Eq. (9) over the mesh Q_{i_R} in space along with using the integration by parts formula and interior condition (6),

$$\begin{aligned}\int_{Q_{i_R}} P(t_{n+1},V)\,dV - \int_{Q_{i_R}} P(t_n,V)\,dV - \int_{t_n}^{t_{n+1}} D\partial_V P(t,V_{i_R+\frac{1}{2}}) - D\partial_V P(t,V_{i_R-\frac{1}{2}})\,dt \\ = -\int_{t_n}^{t_{n+1}} \left[D\partial_V P(t,V^R)\right]dt \qquad = \qquad -\int_{\max(0,t_n-\tau_R)}^{\max(0,t_{n+1}-\tau_R)} D\partial_V P(t,V^T)\,dt\ .\end{aligned} \tag{22}$$

For all $t\in(t_n,t_{n+1}]$, the diffusive flux across V^T, $D\partial_V P(t,V^T)$, is approximated by $\mathscr{B}_{N+\frac{1}{2}}^{n+1}$ in Eq. (21), so the numerical diffusive flux across V^T is defined for all $t\in\mathbb{R}_+$ by the piecewise constant function

$$F(t) = \sum_{n=0}^{+\infty} \mathscr{B}_{N+\frac{1}{2}}^{n+1}\chi_{(t_n,t_{n+1}]}(t) = -\sum_{n=0}^{+\infty} 2D\frac{P_N^{n+1}}{\Delta V_N}\chi_{(t_n,t_{n+1}]}(t), \tag{23}$$

where $\chi_{(t_n,t_{n+1}]}$ denotes the characteristic function on $(t_n,t_{n+1}]$. Then, we discretize Eq. (22) by

$$\Delta V_{i_R}P_{i_R}^{n+1} - \Delta t(\mathscr{B}_{i_R+\frac{1}{2}}^{n+1} - \mathscr{B}_{i_R-\frac{1}{2}}^{n+1}) = \Delta V_{i_R}P_{i_R}^{n+\frac{1}{2}} - \int_{t_n-\tau_R}^{t_{n+1}-\tau_R} F(t)\,dt\ , \tag{24}$$

where the numerical fluxes $\mathscr{B}_{i_R\pm\frac{1}{2}}^{n+1}$ are given again by (20), as the value of $P(t,V^R)$ is well defined under the continuity condition (5).

Note that $F(t)=0$ when $t<0$ by definition (23), so that the mass will be re-injected at V^R only after $t_{n+1}>\tau_R$. Also, notice that $(t_n-\tau_R,t_{n+1}-\tau_R)$ may not agree with any of the preceding sub-intervals (t_k,t_{k+1}) where $k\le n$ (See Fig. 2).

2.4. Summary of the finite volume method

As the numerical method described above is somewhat technical, we give a brief summary and state the main result of this paper. An approximate solution of system (2–6) is found in two steps:

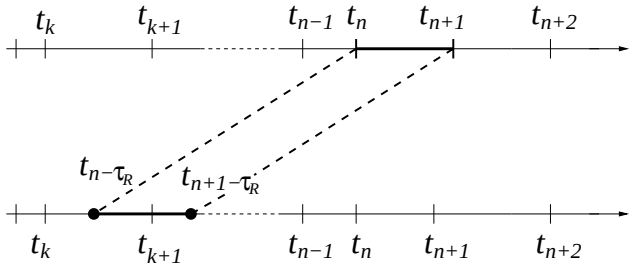

Figure 2. A schematic illustration of the discretization of condition (6). The mass crossing the threshold during $(t_n - \tau_R, t_{n+1} - \tau_R)$ is re-injected at V^R after the refractory period τ_R.

1. Assuming that P^n is known, we solve the pure drift problem (8), with boundary conditions $P(t,0) = P(t,V^T) = 0$, $t \in (t_n, t_{n+1})$. This problem actually has a unique viscosity solution. We define $P^{n+\frac{1}{2}}$ as the numerical solution at time t_{n+1} given by the explicit scheme (11), where the numerical fluxes, $\mathscr{A}^n_{i+\frac{1}{2}}$, are given by (12) in the interior, that is, if $i \neq 0, N$, and by $\mathscr{A}^n_{\frac{1}{2}} = \mathscr{A}^n_{N+\frac{1}{2}} = 0$ on the boundary.

2. Using the updated numerical solution $P^{n+\frac{1}{2}}$, as an initial condition we then solve the pure diffusion equation (9) on (t_n, t_{n+1}) with boundary conditions $D\partial_V P(t,V^\infty) = 0$, $P(t,V^T) = 0$ and interior conditions (5–6). This is accomplished by using the implicit scheme (19) for all $i \neq i_R$, and (24) for $i = i_R$ (that means, in the mesh containing the reset potential). The numerical fluxes are given by Eq. (20) if $i \neq 0, N$. The boundary conditions are handled by defining $\mathscr{B}^{n+1}_{\frac{1}{2}} = 0$, and using Eq. (21) when $i = N$. Therefore, in this second step P^{n+1} is obtained from $P^{n+\frac{1}{2}}$ by solving a linear system whose matrix is strongly column diagonally dominant, as described in Fig. 3, and is consequently invertible. Notice that if $\Delta t_n > \tau_R$, which is indeed true if $\tau_R = 0$, the term $\int_{t_n-\tau_R}^{t_{n+1}-\tau_R} F(t)\,dt$ contains an implicit term, $\int_{t_n}^{t_{n+1}-\tau_R} F(t)\,dt = -2D\frac{(\Delta t_n - \tau_R)}{\Delta V_N} P^{n+1}_N$, that must be taken into account in the matrix. Moreover, to optimize storage disk space and computation time, we only store and manipulate the coefficients of the matrix that are different from 0, which means, the three main diagonals and -2β. The inversion of this system is carried out by a standard gradient procedure accelerated by incomplete LU preconditioning (Lascaux and Théodor, 1987; Press et al., 2007).

The following proposition is the main result of this paper. The proof is given in Appendix B.

PROPOSITION 2. *Under conditions (15–16), the overall operator splitting method (10) is nonnegativity preserving and satisfies the mass balance stability condition:*

$$\|P^n\|_{l^1} = \|P^0\|_{l^1} + \int_{t_n-\tau_R}^{t_n} F(t)\,dt\ , \tag{25}$$

where F is defined by (23).

REMARK 2. The property of the solution given by Eq. (25) is a discrete counterpart of (7) and makes our method l^1–stable. On the other hand property (17) implies that no spurious extrema due to the drift are created.

Figure 3. Diffusion matrix with $\alpha_{i+\frac{1}{2}} = D\frac{\Delta t_n}{\Delta V_{i+\frac{1}{2}}}$ and $\beta = D\frac{\max(0,\Delta t_n - \tau_R)}{\Delta V_N}$.

2.5. MONTE CARLO SIMULATIONS AND ANALYTICAL SOLUTIONS

We compared the densities obtained using the above numerical method with those obtained using Monte Carlo (MC) simulations, and, when available, analytical results. In all cases tested, we simulated an ensemble of 10^6 neurons with initial condition $V(0)$ sampled from a uniform distribution. Numerical solutions to the stochastic differential equation corresponding to Eq. (1) were computed using the Euler–Maruyama method (Kloeden and Platen, 1992). When the potential of a neuron exceeded V^T, it was reset to V^R and pinned to this value for a period τ_R. A snapshot of all 10^6 values of V was taken at different time points to obtain an estimate of $P(t,V)$. Neurons in the refractory period were not included in the figures showing the densities. All MC simulations were performed in Matlab. A separate implementation in C++ was used to check the results. This implementation resulted in a reduction of integration time of at most a factor of 2.

The stationary distribution for the LIF model as a function of input current, noise intensity and refractory period can be found in (Burkitt, 2006; Lindner, 2001). The integral in the expression was integrated numerically using the *quadl* function in Matlab.

3. Results

We show that even with modest grid sizes and average computational resources our method produces results of very good accuracy in very short computational time. The method was tested using the LIF and QIF model with and without refractory period, τ_R.

The domain used in the finite volume method was $(-100,1)$, so that $V^\infty = -100$ and threshold voltage $V^T = 1$. The threshold voltage was set to $V^R = 0$, so that the domain was large. Therefore, the artificial reflecting boundary at V^∞ did not significantly affect solutions in the region of interest near V^R and V^T.

The interval $(-1,1)$ is partitioned into 101 subintervals as follows: the intervals $(-1,-0.02)$ and $(0.02,1)$ are both partitioned into 49 subintervals of equal size, while $(-0.02,0.02)$ is split into 3 subintervals of equal size. This way, the reset potential falls exactly on V_{51}. For efficiency, the interval $(-100,-1)$ is partitioned into only 10 subintervals of equal size. We assumed that the numerical solution has reached its stationary state when $\|P^{n+1} - P^n\|_{l^\infty} \leq \varepsilon$, where we chose $\varepsilon = 10^{-6}$ in practice.

All simulations were run on an average desktop computer. As the runtimes will be dependent on architecture, memory and implementation, we do not report the exact numbers here. We just note that the finite volume scheme runs in a fraction of a second to a couple seconds on our machines. This is typically an improvement of three to four orders of magnitude over the MC simulations.

3.1. Leaky integrate and fire model (LIF)

We start by considering the classical stochastic LIF model, described by Eq. (1) with $f(V) = -V + \mu$. The corresponding probability density evolves according to Eqs. (2–6). Here, μ is a fixed parameter that describes the direct component, or bias, of the input current. . The value of μ also gives the equilibrium point of the deterministic equation obtained by setting $D = 0$ in Eq. (1). If $\mu < 1$, then the cell fires only due to input fluctuations, and is thus in the *fluctuation dominated regime*. When $\mu > 1$, threshold crossings are, at least in part, due to drift.

We simulated neurons in the fluctuation driven regime ($\mu = 0.5$), as well as the drift dominated regime ($\mu = 1.5$), with both small and large noise, resulting in four test cases. The parameter values used in each test are summarized in Table 3.1. In all cases the initial distribution was uniform on the interval $(0.08, 0.1)$, resulting in long convergence times for some of the tests.

	Test 1	Test 2	Test 3	Test 4
μ	0.5	0.5	1.5	1.5
D	0.01	0.1	0.01	0.1

Figure 4. LIF: value of the parameters. Here $\mu = 0.5$ corresponds to the fluctuation dominated case, and $\mu = 1.5$ to the drift dominated regime. The noise is considered to be low if $D = 0.01$ and high if $D = 0.1$.

We first compare the steady state solution obtained numerically with the exact analytical expression. We present the results of tests 2 and 4 in Fig. 5, and similar agreement was found in all other cases tested.

The numerical approximations of $P(t,V)$ at different times, obtained by the finite volume and MC method are shown in Fig. 6. The finite volume solution is accurate and remains nonnegative and non-oscillatory. The numerical solutions converge in time towards their steady states shown in the right column of Fig. 6.

To observe how the refractory period is captured by the finite volume method, we repeat Test 3 again with $\tau_R = 0$ and compare the numerical solution with that obtained previously for $\tau_R = 0.2$. As shown in Fig. 7,

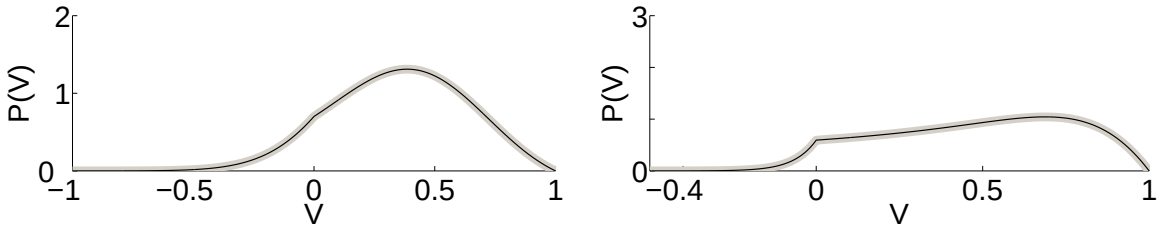

Figure 5. Comparison of numerical and analytical steady state solutions in test cases 2 and 4. In all cases tested, the two solutions were not distinguishable by eye. We therefore present the numerical solution as a thick, gray, transparent line. The analytical solution, in black, is superimposed. The refractory period is $\tau_R = 0$

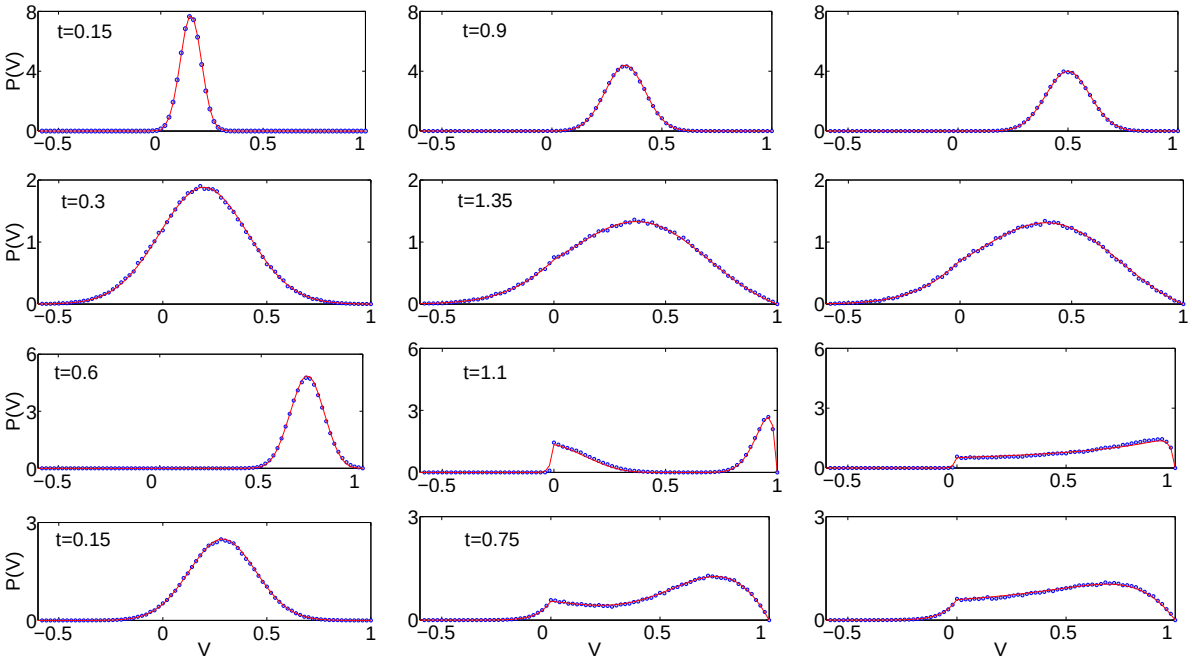

Figure 6. The stochastic LIF model: Numerical solution at different times steps (left and middle column) and steady-state (right column) numerical solution for Tests 1–4, from top (Test 1) to bottom (Test 4); the solid line is the finite volume solution, the dotted line is the MC solution. The refractory period is $\tau_R = 0.2$. Error bars for the MC solution are approximately the size of the dots, and are therefore not shown.

the flux across V^T is instantly re-injected at the reset V^R if $\tau_R = 0$. The re-injection has not yet occurred at $t = 0.8$ in the case $\tau_R = 0.2$.

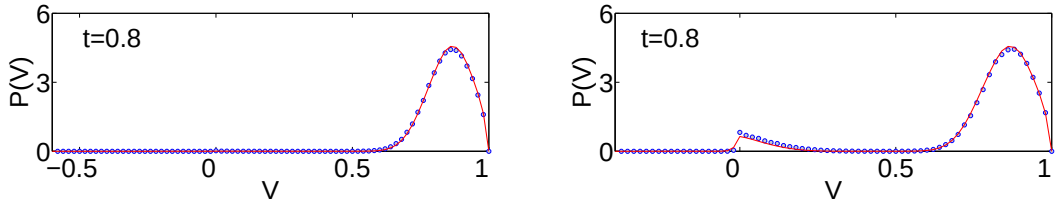

Figure 7. LIF: Numerical solution for Test 3 with refractory period $\tau_R = 0.2$ (left) and $\tau_R = 0$ (right); the dotted line is the MC solution, the solid line is the finite volume solution.

3.2. QUADRATIC INTEGRATE AND FIRE MODEL (QIF)

To illustrate the performance of the code with a different drift operator, we consider the QIF model where, $f(V) = (V - V_1)(V - V_2) + \mu$. Here $0 < V_1 < V_2 < 1$ and μ are three real parameters.

If $0 < \mu < \frac{1}{4}(V_1 - V_2)^2$ then the deterministic system corresponding to Eq. (1) with $D = 0$ has two fixed points in $(0,1)$. Again, the stochastic system can cross threshold only in response to input fluctuations. The deterministic counterpart to system (1) undergoes a saddle node bifurcation as μ crosses $\frac{1}{4}(V_1 - V_2)^2$. Therefore, for $\mu > \frac{1}{4}(V_1 - V_2)^2$ there are no fixed points in $(0,1)$ and threshold crossings are, in part, due to drift (Ermentrout and Kopell, 1986).

We define Test 5 by setting $V_1 = 0.1$, $V_2 = 0.9$, $\tau_R = 0.2$, $\mu = 0.15$, $D = 0.1$. The initial condition is the uniform distribution on $(0.48, 0.5)$ in both cases. As shown in Fig. 8 the finite volume method gives a very good approximation of the probability density at different times.

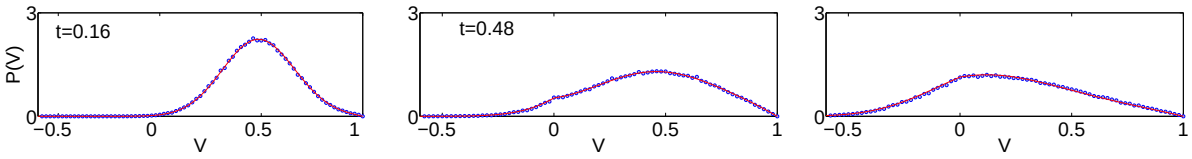

Figure 8. QIF: Numerical solution at different times (left and middle) and the steady-state solution (right) obtained using the finite volume method (solid line) and MC simulation (dots). The refractory period is $\tau_R = 0.2$

3.3. TIME DEPENDENT PARAMETERS

We next present an extension of the method to IF models with time dependent drift and noise intensity. We numerically approximate the solution of

$$\partial_t P(t,V) + \partial_V \big(f(t,V)P(t,V) - D(t)\partial_V P(t,V) \big) = 0.$$

The drift is defined by $f(t,V) = -V + 1 + \frac{1}{2}\sin(2\pi t)$, and the diffusion coefficient varies in time according to $D(t) = 0.01 + 0.09\big|\cos(2\pi t)\big|$. The solution of $f(t,V) = 0$ varies between 0.5 and 1.5, the two values used in Section 3.1. The system therefore switches between diffusion and drift dominated regimes. The diffusion coefficient varies between 0.01 and 0.1.

The interior boundary condition (6) also becomes time-dependent, as $\big[D(t)\partial_V P(t,V^R)\big] = D(t-\tau_R)\partial_V P(t-\tau_R, V^T)$. Therefore, D must be replaced with $D(t_{n+1})$ in (20–21) and (23). The time step may vary to satisfy conditions (15–16). Indeed, the coefficients $f(t_n, V_{i+\frac{1}{2}})$, $D(t_{n+1})$ must now be computed at each iteration. The diffusion matrix (Fig. 3) also has to be updated at each iteration. However, as we only store non-zero coefficients and the structure of the matrix is static, this update only affects the non-zero coefficients by a factor $D(t_{n+1})$. The drift-scheme $\mathscr{S}_1$ is explicit, so the overall complexity of our algorithm is not much affected. The run time is comparable to the constant coefficient case.

When the coefficients are periodic, it is expected that the solution $P(t,V)$ asymptotically becomes periodic in time. Indeed, the snapshots of the numerically obtained solution show that this is the case (see Fig. 9). Finally, in Fig. 10, we observe the match between the firing rate obtained with MC simulation and our finite volume method. For the latter, the firing rate is defined as $-D(t)\partial_V P(t,V)|_{V^T}$, the negative diffusive flux across the boundary V^T. This is approximated for each t_n by $-F(t_n) = D(t_n)\frac{P_N^n}{\Delta V_N/2}$.

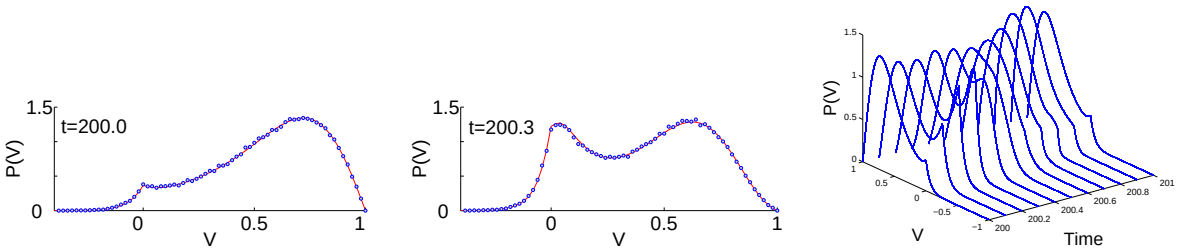

Figure 9. Time dependent stochastic LIF model: The left and middle panels show a comparison between the finite volume solution (solid line) and the MC solution (dotted line) at different times. The right panel shows ten snapshots of the asymptotic time periodic distribution obtained using the finite volume method. The refractory period is $\tau_R = 0.2$

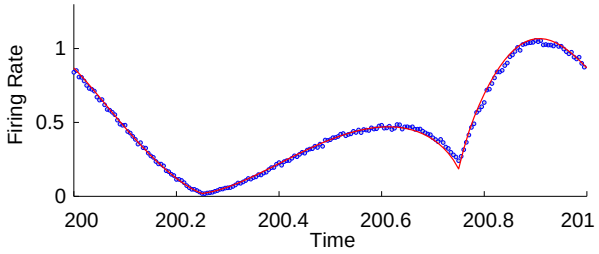

Figure 10. Time dependent stochastic LIF model: Comparison between the numerical firing rates of our finite volume solution (solid line) and MC solution (dotted line) over one period after convergence to a periodic distribution for Test 6. The refractory period is $\tau_R = 0.2$

4. Discussion

We have presented a fast and accurate numerical method for computing solutions of Fokker-Planck equations that frequently arise in theoretical neuroscience. The method involves a two-step operator decomposition which enabled us to cope with the different difficulties separately. The first step involved the discretization of the underlying pure drift equation. Here the use of flux limiters provides numerical densities that are accurate and non-oscillatory at the same time. This is a numerical counterpart of the fact that the exact solution has bounded variations. The second step involved the discretization of the pure diffusion operator and interior boundary conditions by an implicit scheme. An explicit method would require a very restrictive time step condition to obtain nonnegative densities leading to very long run times. As the mass crossing the threshold is accurately re-injected at the reset location there is no loss or gain of mass over time.

The numerical densities obtained by our overall operator splitting technique are proved and observed to be nonnegative and satisfy a discrete mass balance property. Our solutions were tested through six different test-cases against MC simulations and analytical solutions when available. In all cases the agreement was very good.

We note a potential limitation common to all explicit schemes: the time step condition is restricted by the drift operator and the mesh-size. Hence, a refinement in the mesh leads to a decrease in the time step, Δt, and an increase in run time.

However, we do not need a very fine mesh to obtain accurate solutions. The number of mesh-points (110), is much smaller than the number of neurons ($10^5 - 10^6$) needed to obtain similar accuracy using MC simulations. Also, we select CFL ratios given by the left-hand side of (15–16) equal to one in order to maximize the time step. Consequently, our method ran four to five orders of magnitude faster than Monte Carlo simulations.

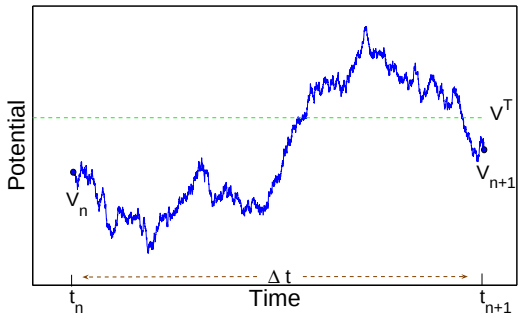

Figure 11. A direct implementation of the Euler–Maruyama method typically underestimates the firing rate of the stochastic IF model. There is always a nonzero probability that between the times t_n and t_{n+1} a sample path has crossed the threshold voltage V^T.

We also note that typical MC simulations will tend to underestimate the probability that a neuron fires during a given time interval. Assuming that an Euler-Maruyama method is used to simulate realizations of the SDE, we see that there will always be a chance that the sample voltage path, $V(t)$, crosses threshold between two time points in the simulation (See Fig. 11). Indeed this probability can be computed using the the reflection principle as

$$Pr[V(t) > V^T \text{ for } t \in (t_n, t_{n+1}) | V(t_n) = V_n, V(t_{n+1}) = V_{n+1}] = \exp\left[-\frac{1}{D\Delta t}[(V^T - V_n)(V^T - V_{n+1})]\right],$$

where t_i are the times at which the solution is approximated, and we assumed constant drift near the boundary. Moreover, the probability mass crossing the threshold is typically assumed to be re-injected exactly at V^R at the end of each time step, leading to a spurious point mass at that location. Although more sophisticated numerical methods can be used to avoid these problems (Kloeden and Platen, 1992), accurate MC simulations typically require very small time steps.

The extension of the present finite volume methods to two and three dimensions does not involve any conceptual difficulties and is the subject of a forthcoming paper. It is indeed in higher dimensions that the time savings and accuracy of the method may have their real impact, as accurate MC simulations of networks of two to three cells can be prohibitively time consuming.

5. Acknowledgements

We thank Cheng Ly, Roberto Fernández Galán and Brent Doiron for helpful discussions. This research was supported by NSF grants DMS-0604429 and DMS-0817649, and a Texas ARP/ATP award.

Appendix

A. Construction of numerical scheme (11–12) and proof of proposition 1

[1]First, consider the second order Taylor expansion

$$P(t_{n+1},V) = P(t_n,V) + \Delta t\,\partial_t P(t_n,V) + \frac{\Delta t^2}{2}\partial_{tt}P(t_n,V) + \mathscr{O}(\Delta t^3)\ . \tag{26}$$

Then, integrating over one cell using $\partial_t P = -\partial_V(Pf)$, $\partial_{tt}P = \partial_V\big(f\partial_V(Pf)\big) = f\partial_{VV}(Pf) + \partial_V f\partial_V(Pf)$ and the integration by parts formula, one has

$$\int_{Q_i} P(t_{n+1},V)\,dV = \int_{Q_i} P(t_n,V)\,dV - \Delta t\Big[P(t_n,.)f\Big]_{V_{i-\frac12}}^{V_{i+\frac12}} + \Delta t^2\Big[f^2\partial_V P(t_n,.) + P(t_n,.)f\partial_V f\Big]_{V_{i-\frac12}}^{V_{i+\frac12}}$$
$$+ \Delta t^2\int_{Q_i}\partial_V f\partial_V(Pf)\,dV + \mathscr{O}(\Delta t^3)\ . \tag{27}$$

For the time being, let us neglect the terms containing Δt^2, so that (26) reduces to the first order Taylor expansion. Then, one of the simplest stable schemes can be derived by using the first order upwind approximation $P(t_n,V_{i+\frac12})f(V_{i+\frac12}) \approx P_i^n f_{i+\frac12}^+ + P_{i+1}^n f_{i+\frac12}^-$ in the first term of the right-hand side of (27). We obtain the numerical scheme (11–12) with $\varphi \equiv 0$, which is first order accurate in space and time. Such accuracy does not properly capture some possible drift effects, such as sharp fronts (see for instance (Bruneau et al., 2005; Godlewski and Raviart, 1990)). It has been observed that using a second order approximation of the space derivatives improves drastically the accuracy of numerical solutions to hyperbolic equations, even if the accuracy in time is still of first order. For this reason, we use instead the centered discretization $P(t_n,V_{i+\frac12})f(V_{i+\frac12}) \approx f_{i+\frac12}\big(\gamma_{i+\frac12}P_i^n + (1-\gamma_{i+\frac12})P_{i+1}^n\big)$ in the first term of the right-hand side of (27), where the coefficient $\gamma_{i+\frac12} = \frac12\frac{\Delta V_{i+1}}{\Delta V_{i+\frac12}}$ interpolates the numerical solution at the interface $V_{i+\frac12}$, thus allowing us to handle variable size mesh elements. Finally, we further improve the accuracy of our scheme by including the term $\Big[f^2\partial_V P(t_n,.)\Big]_{V_{i-\frac12}}^{V_{i+\frac12}}$ and using a centered approximation, $f^2(V_{i+\frac12})\partial_V P(t_n,V_{i+\frac12}) \approx f_{i+\frac12}^2\frac{P_{i+1}^n - P_i^n}{\Delta V}$ for all i. This results in the numerical scheme (11–12) with $\varphi \equiv 1$, which is more accurate in space and time than the upwind scheme, but unstable. Also notice that it becomes second order accurate in time if the drift term is constant, hence cancelling out the terms containing $\partial_V f$ in Eq. (27).
Indeed, the flux (12) is a perturbation of the upwind scheme, so a compromise between accuracy and stability is offered by selecting φ satisfying (13).

In order to prove Proposition 1, the resulting scheme (11–12) is written as $P_i^{n+\frac12} = P_i^n\Big(1-\Delta t\frac{f_{i+\frac12}-f_{i-\frac12}}{\Delta V_i}\Big) + A_{i+\frac12}^n\Delta P_{i+\frac12}^n - B_{i-\frac12}^n\Delta P_{i-\frac12}^n$, with

$$A_{i+\frac12}^n = -\frac{\Delta t\,f_{i+\frac12}^-}{\Delta V_i}\left(1-\frac12\Big(1+\frac{\Delta t\,f_{i+\frac12}^-}{\Delta V_{i+1}}\Big)\frac{\Delta V_{i+1}}{\Delta V_{i+\frac12}}\phi_{i+\frac12}^m + \frac12\Big(1+\frac{\Delta t\,f_{i-\frac12}^-}{\Delta V_i}\Big)\frac{\Delta V_i}{\Delta V_{i-\frac12}}\frac{\phi_{i-\frac12}^m}{r_{i-\frac12}^m}\right),$$
$$B_{i-\frac12}^n = \frac{\Delta t\,f_{i-\frac12}^+}{\Delta V_i}\left(1-\frac12\Big(1-\frac{\Delta t\,f_{i-\frac12}^+}{\Delta V_{i-1}}\Big)\frac{\Delta V_{i-1}}{\Delta V_{i-\frac12}}\phi_{i-\frac12}^p + \frac12\Big(1-\frac{\Delta t\,f_{i+\frac12}^+}{\Delta V_i}\Big)\frac{\Delta V_i}{\Delta V_{i+\frac12}}\frac{\phi_{i+\frac12}^p}{r_{i+\frac12}^p}\right).$$

Using property (13) and re-phrasing

$$P_i^{n+\frac12} = P_i^n\Big(1-\frac{\Delta t}{\Delta V_i}(f_{i+\frac12}-f_{i-\frac12})^+ - A_{i+\frac12}^n - B_{i-\frac12}^n\Big) - \frac{\Delta t}{\Delta V_i}(f_{i+\frac12}-f_{i-\frac12})^- P_i^n + A_{i+\frac12}^n P_{i+1}^n + B_{i-\frac12}^n P_{i-1}^n\ ,$$

[1] I modified the proof

one has $A^n_{i+\frac{1}{2}} \geq 0$, $B^n_{i-\frac{1}{2}} \geq 0$ and $1 - \frac{\Delta t}{\Delta V_i}(f_{i+\frac{1}{2}} - f_{i-\frac{1}{2}})^+ - A^n_{i+\frac{1}{2}} - B^n_{i-\frac{1}{2}} \geq 0$ under conditions (15) and (16), implying that the scheme (11–12) is nonnegativity preserving and l^∞–stable.

B. Proof of Proposition 2

Recursively assuming that $P^n_i \geq 0$ for a given index n and all i, which is true for $n = 0$, Proposition 1 and boundary condition $\mathscr{A}^n_{\frac{1}{2}} = 0$, $\mathscr{A}^n_{N+\frac{1}{2}} = 0$ imply that $P^{n+\frac{1}{2}}_i \geq 0$ for all i under conditions (15–16). Then, multiplying (11) by ΔV_i and summing from $i = 1$ to $i = N$, one has $\|P^{n+\frac{1}{2}}\|_{l^1} = \|P^n\|_{l^1}$.
Next, P^{n+1} is obtained by inverting the linear system $MP^{n+1} = S$ whose matrix M is given in Fig. 3 and the right-hand side S is defined by $S_i = \Delta V_i P^{n+\frac{1}{2}}_i$ if $i \neq i_R$, and $S_{i_R} = \Delta V_{i_R} P^{n+\frac{1}{2}}_{i_R} - \int_{t_n-\tau_R}^{\min(t_{n+1}-\tau_R, t_n)} F(t)\,dt$.
Indeed, the matrix M is strongly column diagonally dominant with positive diagonal coefficients and non-positive off-diagonal coefficients. So it is invertible and M^{-1} is a positive matrix. Since the right-hand side S has nonnegative entries, the solution of the system, P^{n+1}, is component-wise nonnegative.
Finally, sum (24) and (19) from $i = 1$ to $i = N$ to obtain

$$\|P^{n+1}\|_{l^1} = \|P^{n+\frac{1}{2}}\|_{l^1} + \int_{t_n}^{t_{n+1}} F(t)\,dt - \int_{t_n-\tau_R}^{t_{n+1}-\tau_R} F(t)\,dt\ ,$$

thus recursively implying (25).

References

Apfaltrer, F., C. Ly, and D. Tranchina: 2006, 'Population density methods for stochastic neurons with realistic synaptic kinetics: Firing rate dynamics and fast computational methods'. *Network-Comp. Neural* **17**(4), 373–418.

Barth, T. and M. Ohlberger: 2004, 'Finite volume methods: foundation and analysis'. *Encyclopedia of Computational Mechanics*.

Bruneau, C. H., F. Marpeau, and M. Saad: 2005, 'Numerical simulation of the miscible displacement of radionuclides in a heterogeneous porous medium'. *Int. J. Numer. Meth. Fl.* **49**(10), 1053–1085.

Brunel, N., F. S. Chance, N. Fourcaud, and L. F. Abbott: 2001, 'Effects of synaptic noise and filtering on the frequency response of spiking neurons'. *Phys. Rev. Lett.* **86**, 2186–2189.

Brunel, N. and V. Hakim: 1999, 'Fast global oscillations in networks of integrate-and-fire neurons with low firing rates'. *Neural Comput.* **11**, 1621–1671.

Brunel, N. and P. E. Latham: 2003, 'Firing Rate of the Noisy Quadratic Integrate-and-Fire Neuron'. *Neural Comput.* **15**(10), 2281–2306.

Burkitt, A. N.: 2006, 'A Review of the Integrate-and-fire Neuron Model: I. Homogeneous Synaptic Input'. *Biol. Cybern.* **95**(1), 1–19.

Courant, R., K. Friedrichs, and H. Lewy: 1928, 'Uber die partiellen Differenzengleichungen der mathematischen Physik'. *Mathematische Annalen* **100**(1), 32–74.

Doiron, B., M. J. Chacron, L. Maler, A. Longtin, and J. Bastian: 2003, 'Inhibitory feedback required for network oscillatory responses to communication but not prey stimuli.'. *Nature* **421**(6922), 539–43.

Ermentrout, G. B. and N. Kopell: 1986, 'Parabolic bursting in an excitable system coupled with a slow oscillation'. *SIAM J. Appl. Math.* **46**(2), 233–253.

Galán, R. F., G. B. Ermentrout, and N. N. Urban: 2007, 'Stochastic dynamics of uncoupled neural oscillators: Fokker-Planck studies with the finite element method'. *Phys. Rev. E* **76**(5), 56110.

Gardiner, C. W.: 1985, *Handbook of Stochastic Methods*. Springer New York.

Godlewski, E. and P. A. Raviart: 1990, *Hyperbolic systems of conservation laws*, Vol. 3/4 of *Mathématiques et applications*. Ellipses.

Harten, A.: 1983, 'High resolution schemes for Hyperbolic Conservation Laws'. *J. Comp. Phys.* pp. 357–392.

Kloeden, P. E. and E. Platen: 1992, *Numerical Solution of Stochastic Differential Equations*. New York, NY: Springer.

Lapicque, L.: 1907, 'Recherches quantitatives sur l'excitation electrique des nerfs traitee comme une polarisation'. *J. Physiol. Path. Gen. (Paris)* **9**, 622–635.

Lascaux, P. and R. Théodor: 1986-1987, *Analyse Numérique Matricielle Appliquée à l'Art de l'Ingénieur*, Vol. 1,2. Masson.

Latham, P. E., B. J. Richmond, P. G. Nelson, and S. Nirenberg: 2000, 'Intrinsic Dynamics in Neuronal Networks. I. Theory'. *J. Neurophysiol.* **83**(2), 808–827.

Lindner, B.: 2001, 'Coherence and stochastic resonance in nonlinear dynamical systems'. Ph.D. thesis, Humboldt University.

Lindner, B. and A. Longtin: 2006, 'Comment on "Characterization of Subthreshold Voltage Fluctuations in Neuronal Membranes" by M. Rudolph and A. Destexhe'. *Neural Comput.* **18**(8), 1896.

Lindner, B. and L. Schimansky-Geier: 2001, 'Transmission of noise coded versus additive signals through a neronal ensemble'. *Phys. Rev. Lett.* **86**, 2934– 2937.

Marpeau, F. and M. Saad: 2007, 'Three dimensional simulation of radionuclide transport in porous media'. *submitted*.

Mattia, M. and P. Del Giudice: 2002, 'Population dynamics of interacting spiking neurons'. *Phys. Rev. E* **66**(5), 51917.

Mattia, M. and P. Del Giudice: 2004, 'Finite-size dynamics of inhibitory and excitatory interacting spiking neurons'. *Phys. Rev. E* **70**(5), 52903.

Press, W. H., S. A. Teukolsky, W. T. Vetterling, and B. P. Flannery: 2007, *Numerical Recipes: The Art of Scientific Computing, 3rd Edition*. Cambridge University Press.

Rall, W.: 1995, *The Theoretical Foundation of Dendritic Function: Selected Papers of Wilfrid Rall with Commentaries*. Boston, MA: MIT Press.

Renart, A., N. Brunel, and X. J. Wang: 2004, 'Mean-field theory of irregularly spiking neuronal populations and working memory in recurrent cortical networks'. In: *Computational neuroscience: A comprehensive approach*. Boca Raton, FL: Chapman & Hall, pp. 431–490.

Risken, H.: 1989, *The Fokker-Planck equation: Methods of Solution and Applications*. Springer-Verlag Berlin and Heidelberg GmbH & Co. K.

Roe, P. L.: 1984, 'Generalized formulation of TVD Lax-Wendroff schemes'. *ICASE Rep.* pp. 53–84.

Rudolph, M. and A. Destexhe: 2005, 'An Extended Analytic Expression for the Membrane Potential Distribution of Conductance-Based Synaptic Noise'. *Neural Comput.* **17**(11), 2301–2315.

Strang, G.: 1968, 'On the construction and comparison of difference schemes'. *SIAM J. Numer. Anal.* **5**, 506–517.

Sweby, P. K.: 1984, 'High resolution schemes using flux limiters for hyperbolic conservation laws'. *SIAM J. Numer. Anal.* pp. 995–1011.

Toro, E. F.: 2001, *Godunov Methods: Theory and Applications*. Kluwer Academic/Plenum Publishers.

Tuckwell, H. C.: 1988, *Introduction to Theoretical Neurobiology*. Cambridge, UK: Cambridge University Press.

Tuckwell, H. C.: 1989, *Stochastic Processes in the Neurosciences*. Philadelphia, PA: SIAM.